NASA Contractor Report 188357

Burn Rates of TiH2/KClO4/Viton and Output Testing of NASA SKD26100098-301 Pressure Cartridges

John A. Holy

EG&G Mound Applied Technologies

National Aeronautics and
Space Administration

1993

N95-15715

Unclas

G3/25 0031027

(NASA-CR-188357) BURN RATES OF TiH2/KClO4/VITON AND OUTPUT TESTING OF NASA SKD26100098-301 PRESSURE CARTRIDGES (EG and G Mound Applied Technologies) 50 p

Table of Contents

ABSTRACT

The burn rates of the pyrotechnic $TiH_2/KClO_4/Viton$ with a mass ratio of 30/65/5 have been measured as a function of pressure in nitrogen up to 312 MPa(45 Kpsi). The burn rates were fit to $R = a P^n$, with $a = 2.055$ cm/sec/MPa^n and $n = 0.472$ between 0.15 MPa (22 psi) and 21.6 MPa (3.13 Kpsi) and $a = 4.38$ cm/sec/MPa^n and $n = 0.266$ between 70 MPa (10.15 Kpsi) and 312 MPa (45.25 Kpsi). The decrease in slope at the higher pressures is attributed to a diffusion limited reaction. No acoustically driven flame instabilities or large conductive-to-convective burn transitions were observed. Solid reaction products were analyzed by x-ray diffraction and scanning electron microscopy (SEM). X-ray diffraction detected only TiO_2 and KCl. SEM showed that the particle size of the reaction products increased as the nitrogen pressure increased. There were no anomalous characteristics of the burn of this pyrotechnic that could be interpreted as a cause of the o-ring blow-by problem in the forward shear bolt assembly.

Three NASA SKD26100098-301 pressure cartridges were fired into a fixed volume vessel that was sealed with an O-ring. A maximum pressure of 181.7 MPa(26,350 psi) was reached in around 100 μsec for two shots fired into a volume of 16.3 cm^3(0.996 in^3). A maximum pressure of 33,460 psi was reached for one shot fired into a volume of 9.55 cm^3(0.583 in^3). The O-ring burned through on one shot in the larger volume and leaked on the other two thereby simulating the effects of an O-ring leak. The results imply that the piston in the shear bolt assembly would receive a large impulse even if there was a leak in an O-ring seal.

INTRODUCTION

The work reported here was initiated at the request of NASA to learn more about the functioning of a shear bolt assembly used on the space shuttle. The $TiH_2/KClO_4/Viton$ pyrotechnic in two SKD26100098-301 pressure cartridges drives a piston which shears a bolt that holds the external fuel tank to the shuttle. The piston is sealed along its side by two O-rings. In about 30% of the recovered shear bolt assemblies, the O-rings have been burned through. It was this O-ring burn-through that increased the need to learn more about the functioning of the shear bolt assembly. A detailed description of the shear bolt assembly and O-ring burn-through occurs in a companion report by Reed.[1] Reed's report is a theoretical analysis of the pyrotechnic burn and its effect on the functioning of the shear bolt assembly. This report is an experimental study of the burn properties of the pyrotechnic and of the pressure output of the cartridges used in the shear bolt assembly.

INTRODUCTION TO BURN RATES

Burn rate measurements can provide important information about the characteristics of propellants, pyrotechnics, and explosives. There has been extensive use of burn rate data in the propellant industry for many years, and it is a straightforward matter to apply the techniques developed for propellants to pyrotechnics and explosives. A pyrotechnic may be considered a heterogeneous propellant and an explosive a homogeneous propellant when

burned in a normal propellant-type configuration. In fact, some secondary explosives are used in propellant formulations.

The two most commonly used methods to measure burn rates are the closed bomb technique and the strand burner technique. Juhasz and Price[2] have given a general review of the closed bomb technique. Kubota[3] has reviewed pressure-dependent burn rates in the context of rocket propellants.

In the usual closed bomb technique, a pressure bomb is loaded with propellant grains at a typical density of 0.1 to 0.2 gm/cm^3. With this amount of propellant in the bomb, the product gases and heat generated by the burning sample will raise the bomb pressure from atmospheric to 350 to 700 MPa (50 to 100 Kpsi). From the pressure-time record of only one burn, the burn rate as a function of pressure over the total pressure range may be calculated. However, the calculations are often complex, involving equations of state, thermochemistry, geometrical factors of the propellant grains, and heat losses to chamber walls with assumptions such as uniform ignition of all grain surfaces and constant regression of grain surfaces at each pressure.[2,4]

In the strand burner technique, the sample is pressed into a strand and two or more fuse wires are placed in the sample at known intervals. The pressure bomb is pressurized with an inert gas, normally nitrogen, and its volume is large relative to the sample mass so that the sample burns in an approximately constant pressure environment. The fuse wire breaks measure the passing of the flame front, and the time interval between breaks directly determines the burn rate at one pressure. There are no complex calculations or assumptions involved, but many samples are required to determine the burn rate over a large pressure range. More recently, Constantino, Ornellas, and Tao[5,6] have used a hybrid closed bomb-strand burner in which more than a dozen fuse wire breaks are used to determine burn rates over a large pressure range as a long strand of explosive burns and increases the pressure in the closed bomb.

The burn rates determined in our experiments were obtained from a different type of hybridization. Small samples were burned in a bomb pressurized with nitrogen as in a strand burner, but the burn rates were determined from the small pressure pulse generated during the burn as in the closed bomb technique. Thus, the sample burned under approximately constant pressure conditions as in the strand burner, but a continuous record of the burn is obtained rather than just a few timing marks. This continuous record is important when deviations from a constant burn rate at an approximately constant pressure occur.

Burn rates are usually fit to the empirical de St. Robert or Vieille's equation

$$R = aP^n, \tag{1}$$

where R is the burn rate, P the pressure, and a and n constants determined from the best fit. The amount of pressure dependence for a composition is usually considered indicative of the degree of involvement of gas phase reactions in the burn. A truly gasless system may show no dependence of the burn rate on pressure, or even a decreasing burn rate with increasing pressure as the high pressure gas acts as a heat sink. Many explosives typically have values of n in the 0.8-1 range up to 350 MPa while values of n determined for pyrotechnics are in the 0.2-0.4 range up to 3 MPa.[7-13] The burn rates of these pyrotechnics usually become

constant or decrease as the pressure is further increased. Most of the burn rate data on pyrotechnics has been obtained at pressures below 20 MPa.

The fitting parameters a and n are also analytical numbers that are associated with a given batch of material. Thus, the burn rate fit can also be used as a quality control tool to monitor for any variations in batch-to-batch performance, with n generally being the index used for comparison.[2]

The burn rates of similar pyrotechnic mixtures, $TiH_x/KClO_4$(x=0.2, 0.65, 1.65), have previously been measured up to 350 MPa.[14] The measurements reported here are essentially a repetition of these previous experiments using the $TiH_2/KClO_4$/Viton pyrotechnic composition.

BURN RATE EXPERIMENTAL

Lot TR120591 from OEA, Denver, Colorado was used for the burn rate measurements. Its composition is $TiH_2/KClO_4$/Viton with a mass ratio of 30/65/5. The TiH_2 and $KClO_4$ have nominal particle sizes of 2 microns and 13 microns, respectively. Viton is a binder with chemical composition $(C_5H_{3.5}F_{6.5})_n$[15].

The powder was pressed into small 316 stainless steel charge holders in two increments with a pressing pressure of 42.34 MPa (6140 psi), the same as used in the NASA cartridge. The charge holders have a length of 0.61 cm and an inner diameter of 0.305 cm. A typical sample mass is approximately 90 mg at a density of 2.1 gm/cm^3.

Figure 1 shows the configuration used to measure the burn rates. The pressed powder in a charge holder is mounted on the cover of the pressure bomb, a model R1.5-6-60 from High Pressure Equipment Company, Inc. A Kistler 207C pressure transducer is mounted in the side of the bomb to measure the change in pressure generated by the burning sample. An empty bomb has an inner diameter of 3.81 cm and a depth of 15.24 cm with a volume of 166 cm^3. With the sample and inserts installed, it is estimated from their dimensions that the inner volume of the bomb is approximately 147 cm^3. The top of the pressure bomb is connected through filters, tubing, and remotely operated valves to a pressure system capable of generating 350 MPa.

Most samples were ignited with an ignition wire made from 0.05 mm diameter Tophet C held in contact with the sample surface by a small piece of high temperature tape. An ignition current pulse of 3 amperes for 3 milliseconds was used. However, when initial pressures in the bomb were below about 0.2 MPa, absolute (30 psia), the powder would not ignite even with 30 millisecond pulses. The ignition wire would tend to melt between the sample and electrical feedthrough, but a darkened burn mark could be seen on the sample where it was in contact with the wire. At these lower pressures, an M104 electric match from ICI Americas, Inc. was used to ignite the samples.

The following procedure is used to generate the pressure pulse from the burning sample. The bomb and pressure system is evacuated with a mechanical vacuum pump and then pressurized with nitrogen gas to the desired pressure. The sample is ignited, and the change in pressure is detected by the pressure transducer, amplified by a Kistler 504E amplifier, recorded on an Analogic Data Precision 6000A waveform recorder, and stored on floppy disk.

The pressure bomb, transducer amplifier, and pressure generating equipment are located remotely in a room with a blowout wall, interlocks, and heavy duty door. The controls for operating the pressure equipment, waveform recorder, and firing circuitry are located outside of the room.

BURN RATE RESULTS AND DISCUSSION

Pressure Traces

An ideal pressure trace would result when the whole surface of the pellet is instantaneously ignited and a thin planar flame front proceeds down the sample at a constant rate. The increase in pressure would then be a linear function of time with definite burn start and ending points being easily discernable from slope changes. Robertson and Igel[16] optically measured the burn rate across the surface of a $TiH_{.68}/KClO_4$ pellet pressed against a transparent header and obtained a value of 2.2×10^4 cm/sec, which is about three orders of magnitude larger than the highest burn rates measured for $TiH_2/KClO_4/Viton$. Thus, the assumption of a planar burn front should be valid.

Three pressure traces in the intermediate pressure regime are shown in Figure 2. Most traces are reasonably linear over a large part of the burn. The slight rise in pressure after completion of a burn is attributed to hot reaction products transferring heat to the bomb gas. Definite starting and ending points of the burns can be easily determined from the pressure traces.

Other typical pressure traces in other pressure regions are shown in Figures 3, 4, and 5. From Figure 4, it can be seen how slowly the pellet burns at the lowest pressures. The oscillations in the pressure traces are due to electrical noise pickup resulting from the long lengths of cable used for remote operation and the high gain settings required in the transducer amplifier. At 15 psia, the slope actually becomes negative during the burn due to condensation of reaction products. However, the end of the burn can be easily seen near 1.2 seconds at the change to a larger negative slope.

In our previous experiments on the $TiH_x/KClO_4$ system, acoustically driven instabilities occurred[14]. They were characterized by high frequency oscillations on the pressure traces. No such oscillations were observed in the $TiH_2/KClO_4/Viton$ system.

Low Pressure Ignition

The pellets were able to be ignited down to 0.1 MPa, absolute(15 psia) in nitrogen gas. The samples could not be ignited in vacuum even with the electric match. The ignition properties of $TiH_2/KClO_4/Viton$ appear to be at least qualitatively similar to those of $TiH_x/KClO_4$, which have been shown to have a strong dependence on pressure.[17,18] Increasing the pressure up to about 2.79 MPa(400 psi) greatly reduces the ignition threshold. It is thought that the pressure confines the initial decomposition products and further exothermic reactions closer to the surface and increases heat transfer in the ignition zone; pressure dependent reaction kinetics could also play a part. The increasing burn rate with pressure also increases the heat transfer rate to the ignition zone.

This pressure dependence of the ignition has a practical application in the ignition of a component. For example, if there is a gap or too much porosity near the ignition point, the initial decomposition products or exothermic reaction products can "vent" away from the ignition zone and extinguish the ignition.[18] However, for the NASA cartridge with the very strong ignition source of the NASA standard initiator, the reaction products from the initiator should provide more than enough pressure to reduce the ignition threshold to its lowest possible value.

Conductive-to-Convective Transitions

Conductive burning is characterized by a conductive heat transfer from the flame front to the adjacent unburned layer of the sample. The flame front propagates in a smooth linear manner by starting a decomposition reaction in the unburned portion of the sample in a layer-by-layer process. Convective burning occurs when hot product gases penetrate the pores of the unburned portion of the pellet and ignite individual particles. This results in the burning of a much larger volume of material in a given time than in conductive burning. Transitions from a conductive to a convective mechanism normally cause an abrupt increase in slope of the pressure-time curve when a sample is burned in a propellant-type configuration. Conductive-to-convective burning transitions have been observed in the $TiH_x/KClO_4$ system[14] and in secondary explosives under self-pressurizing[19,20] and constant pressure burning conditions.[19,21]

The $TiH_2/KClO_4/Viton$ system appears to undergo a mild conductive-to-convection transition when burned from the open surface. A distinct increase in slope in the pressure traces at 207 MPa(30 Kpsi) and 279 MPa(40.4 Kpsi) can be seen in Fig. 5. A less distinct slope increase can be discerned about half-way through the burn in the 310 MPa(45 Kpsi) trace.

It is the conductive-to-convective burning transition that is responsible for the major differences in the burn behavior of an energetic material when it is burned from the open surface under pressure and when it is ignited from a confined side and burned in a confined volume as in the NASA cartridge. In the former configuration, the bomb is first pressurized with an inert gas, and the pores of the material become filled with the pressurizing gas before ignition. In a cartridge-type configuration, there is initially only one atmosphere of pressure in the pores before ignition. A much larger pressure gradient between the hot product gases and pellet pores will exist when the material is ignited, and it is expected that the conductive-to-convective transition will occur at lower pressures and be more intense in the cartridge-type configuration. This effect has been observed in the secondary explosive PETN burned in constant pressure and self-pressurizing conditions.[19] Burn rates of $TiH_x/KClO_4$ in long (12.7 cm) sealed tubes have been measured with a fiber optic-streak camera technique.[22,23,24] The burn rate in this confined configuration was measured to be as large as 760 m/sec, as compared to about 0.5 m/sec in the open surface configuration.

The high pressure inert gas in the pellet pores in the open surface propellant-type burning configuration acts to inhibit the conductive-to-convective transition by reducing the pressure gradient between the hot product gases and the pellet pores. Thus, there is a tradeoff with increasing pressure. The increasing burn rate with increasing pressure causes

the product gases to be generated quicker and increase the pressure gradient, but a higher pressure in the pores decreases the pressure gradient and impedes gas movement through the pores. The conductive-to-convective transition can occur sooner in the burn and be more intense at a lower pressure than at a higher pressure. This can be deduced from the pressure traces in Fig. 5 and was also observed in the $TiH_x/KClO_4$ system[14]. Compaction of the pellet from either the initial gas pressure[5,6] or pressure generated during the burn[24] could also inhibit the conductive-to-convective transition to some degree.

Burn Rates

The determination of burn rates is complicated at many pressures by the deviations from a constant slope as shown in Figures 2-5. In some instances, as indicated by the arrow at the 45 Kpsi trace in Fig. 5, there seem to be two linear sections of the pressure trace. Should one be used for the burn rate at 45 Kpsi? Which one? Possible explanations for such deviations from a constant slope are a weak conductive-to-convective burning transition or inhomogeneities in the sample composition. It was decided to simply use the actual time it took the sample to burn rather than the slopes to determine the burn rate at a given pressure. The actual beginning and end of a sample burn could easily be picked off the pressure traces. This time was divided into the sample length to determine the burn rate. The pressure used for that burn rate was the starting pressure plus half the pressure increase caused by the sample burn, which is the average pressure during the burn. The results of these burn rate determinations are given in Appendix 1.

The burn rate data can be fit to the experimental burn rate equation $R = aP^n$ over two pressure ranges. The fit was obtained by using the commercial software program Statgraphics on a personal computer; this program uses the Marquardt nonlinear regression technique. The results of the fit are shown in Figure 6 and in Table 1. There is a definite break in the burn rate vs pressure slope near 40 MPa(5.8 Kpsi). Similar slope breaks have been observed in $TiH_{0.2}/KClO_4$, $TiH_{0.65}/KClO_4$[14], PbO_2/Si, PbO/Si[8], and $Mg/NaNO_3$[9].

TABLE 1. The results of the burn rate fit to $R = aP^n$ for $TiH_2/KClO_4/Viton$, OEA lot TR120591. The first column shows the pressure range of the data used to obtain the fit.

Pressure Range (MPa)	a (cm/sec/Mpa^n)	a standard error	n	n standard error
0.15 - 21.6	2.055	0.019	0.472	0.004
70 - 312	4.380	0.477	0.266	0.021

As a comparison, the fitting results for $TiH_{1.65}/KClO_4$, which were fit to one line between 0.5 and 350 MPa, are reproduced[14] in Table 2 for measurements that were done in N_2 and He.

TABLE 2. The results of the burn rate fit to $R = aP^n$ for $TiH_{1.65}/KClO_4$ in N_2 and He over the pressure range 0.5 - 350 MPa.

Gas	a (cm/sec/MPa^n)	a standard error	n	n standard error
N_2	1.94	0.15	0.429	0.015
He	2.41	0.29	0.384	0.025

The fitted curve for the low pressure region of $TiH_2/KClO_4/Viton$ has similar fitting parameters to $TiH_{1.65}/KClO_4$. The burn rates for the latter mix were determined with the powder pressed in ceramic charge holders at 69 MPa(10 Kpsi) which could generate slightly different burn rate values when compared to steel charge holders due to differences in the thermal properties of the charge holders and powder density. The burn rates and slope increase as the hydrogen content is reduced in the $TiH_x/KClO_4$ system, which implies that the energy content is reduced as the hydrogen content is increased.

One sample was ignited with the electric match at an initial pressure of 152 MPa(22 Kpsi) to check if this stronger ignition source(stronger compared to the hot wire) would drive the sample into a faster burn. No discernable difference in the pressure trace between hot wire and match ignition was observed.

Burn Rate Theories

Theoretical determinations of burn rates can be quite involved due to the complexity of the chemical, thermal, transport, and physical properties of the energetic materials and the need to take into account the interactions and feedback between these properties. Even the most complete theories contain many simplifications and approximations. Values of many required parameters are not known accurately at high pressures and temperatures. The development of theories for homogeneous[25] and composite[26] propellants have been reviewed.

A first approximation of a solid burning from an unconfined surface is shown in Fig. 7.[27] The solid surface is usually located at $x=0$ and one-dimensional theories developed for the burn. The condensed phase reaction zone can be as thin as a few microns. Energy feedback from the gaseous-phase reaction zone induces processes in the condensed phase to keep the deflagration going. Burning particles could also be present in the gas phase.

The burn rate can be controlled by 1) the rate at which molecules from the condensed phase enter the gas phase, 2) the condensed phase reaction rates, or 3) the gas phase reaction rates. The slowest process generally governs the burn rate. High pressure can change the reaction kinetics and relative importance of these regions.

In the $TiH_x/KClO_4$ system, as with many other metal/oxidizer systems[28,29], a condensed phase controlling factor in the ignition and burn is the oxide layer on the metal particles. Theories postulate that diffusion-controlled growth of a TiO_2 layer adjacent to the

gas-solid interface[30-32] or oxide diffusion into the metal to expose a fresh metal surface[33-37] controls the ignition. Ignition occurs slightly above 500°C. The crystalline $KClO_4$ undergoes a crystalline phase transformation near 300°C and begins to decompose at 400°C. A decomposition product $KClO_3$ melts at 356°C so that it is possible to have liquid $KClO_3$ in the condensed phase.

The gaseous-phase reaction zone can consist of 1) a fizz or primary flame zone, where initial gaseous-phase chemical reactions occur, a 2) dark or induction zone and 3) the luminous or secondary flame zone. Increasing pressure decreases the extent of each of these zones, pushing them all closer to the surface thereby increasing heat conduction and possible gas permeation into the condensed phase. At high enough pressures, the secondary flame can merge into the primary flame. Some energetic materials may not contain a fizz and dark zone, and the luminous flame will be on the condensed phase surface. An impressive color plate of the change in the length of the reaction zones with pressure and flames on the surface for several propellants can be found in reference 3. Photographic experiments on pyrotechnic mixes could provide similar information about its deflagration mechanism. The existence of fizz and dark zones, their lengths, and the relative importance of gas phase reactions could at least be qualitatively deduced.

When a given formulation burns in the absence of external perturbations, the burn rate depends on only two parameters, the pressure P and initial temperature T_o according to[27]

$$R = aP^n/(T_e-T_o)^k, \tag{2}$$

where a, n, T_e, and k are positive constants. T_e is called an explosion temperature. Often, k = 1. The pressure exponent n can be related to the reaction order m by n $=m/2$.[26] The reaction order m can be noninteger for multiple step reactions and can be considered a pseudoaverage reaction order.

From purely condensed-phase considerations, the burn rate can also be expressed as

$$R = B_i exp-E/rT_{is}, \tag{3}$$

where i can refer to the fuel or oxidizer, s refers to the surface temperature T, B is the pre-exponential factor, E is an activation energy, and r is the universal gas constant. Equations (2) and (3) are consistent since increasing the pressure will increase the surface temperature.

The increase in burn rate with pressure for $TiH_2/KClO_4$/Viton indicates that gas phase reactions play a role in the overall deflagration process. The value of n in (1) or (2) below 40 MPa is near 0.5, but it is highly unlikely that a simple one step first order reaction is involved because of the reactions in the condensed phase and gas phase necessary to sustain burning. The decrease in slope in the high pressure regime could be due to a diffusion limited process; at higher pressures, vapors diffuse and mix with more difficulty but chemical reaction rates also increase. Thus, the burn could be kinetically controlled below 40 MPa and diffusion controlled above 40 MPa. The shape of the burn rate plot is consistent with this interpretation.[26] Another possibility for the slope change would be for the reaction kinetics to undergo a change near 40 MPa.

Analysis of Reaction Products

Part way through this series of measurements, it was noticed that the residue of solid reaction products left after a burn appeared different for different initial pressures. At low pressures, the residue was fluffy and was a light-colored bluish-grey. At high pressures, the residue was a dark blue and not fluffy. There also seemed to be more residue at the lower pressures. The residue of a few burns at low and high pressures were collected and analyzed by x-ray diffraction and scanning electron microscopy (SEM) to see if at least some qualitative information could be obtained about the solid reaction products. No attempt was made to determine relative product concentrations because of the somewhat crude method of gathering the products collected on the bomb insert after a burn.

For a 30/65/5 mass ratio of $TiH_2/KClO_4/Viton$, the overall global pyrotechnic reaction involved(ignoring the Viton) may be written as

$$0.60TiH_2 + 0.47KClO_4 \rightarrow 0.60TiO_2 + 0.47KCl + 0.60H_2O + 0.08O_2. \qquad (4)$$

The relative concentration of the reaction products are consistent with the theoretical calculations summarized in Figures 4-6 in Reed's report[1], with TiO_2 and KCl being the major condensed products, H_2O being a major gaseous product, and O_2 being a minor gaseous product.

X-ray diffraction identified the starting fuel as $TiH_{1.924}$. X-ray diffraction also identified only rutile TiO_2 and KCl in the residue with the exception of one sample burned in an initial pressure of 45 psi, which was the lowest pressure with analyzed residue. At that pressure, no titanium oxides were detected. It is possible that the titanium oxides were still there, but were nonstoichiometric, amorphous, or had small crystal dimensions. X-ray diffraction typically cannot detect crystalline components with a concentration less than a few percent.

Some typical SEM's with energy dispersive x-ray analysis (EDAX) are shown in Figures 8 to 11. EDAX can detect elements with atomic number greater than 10. Figure 8 shows the original starting material. Figure 9 shows results for a sample burned in 2.0 MPa (290 psi) of nitrogen. It appears that spherical balls of a titanium oxide have formed with small dispersed KCl particles. The enlarged view in Figure 9d shows that small KCl particles are also spherical with some attached to the larger titanium oxide particles.

Figure 10 shows the residue from the burn at 0.31 MPa (45 psi). Some definite crystalline shapes can be seen in Figure 10a, and coalescence of some titanium oxide particles can be seen in the lower left portion of Figure 10b.

A marked change occurs in the reaction products burned at the higher pressures. Figure 11 shows an example from 143 MPa (20.75 Kpsi). The spherically shaped particles are much larger (note the change in scale), and the EDAX analysis indicates that the spheres now have a large K and Cl content with little titanium. One interpretation of this figure would be that the small KCl particles seen at the low pressures have melted and solidified in a layer around the larger titanium oxide particles. An alternative interpretation would be that the titanium oxide and KCl products are mixed together with the K and Cl being more intense in the EDAX analysis. Figure 12 shows residue from a burn at 310 MPa (45 Kpsi)

where it appears that melted products coalesced and were flattened into platelets by the pressure.

The pressure dependence of the reaction products is consistent with higher temperatures, more confinement, and more product coalescence occurring at the higher pressures. These product analyses indicate that there may be some pressure dependence of the resultant products. The fact that there is less residue at higher pressure may indicate that there have been more gas phase products. X-ray diffraction will only detect crystalline products, and there could be a changing fraction of the products that are amorphous and not identified. The differences in particle sizes and temperatures during the burns could influence the reaction product mix. However, the main cause of the difference in product appearance with pressure appears to be a particle size effect.

Application to Components

Although these burn rate measurements were conducted in the open surface propellant-type configuration, there should be a correlation between any changes seen in burn behavior in this configuration and the confined configuration in a cartridge. Larger values of burn rates or higher pressures generated from the same sample mass of different batches in the pressure bomb measurements imply that the pressure output would increase and the time to that output would decrease in a cartridge. If a strong conductive-to-convective burning transition is observed in a given batch, this would imply that this transition would occur earlier in a cartridge and increase its output pressure. This latter effect has been observed in comparison of different batches of the secondary explosive HMX in experiments at this site; batches which had the conductive-to-convective transition at the lowest pressures in the pressure bomb experiments produced the largest impulse in actuator devices.

Another factor which can increase the pressure output and decrease the time of the burn is the temperature dependence of the burn rate.[3] Small increases in the burn rate with temperature can produce relatively large increases in the pressure output. The high pressure burn rate system is capable of measuring the burn rate of materials at pressures up to 69 MPa(10 Kpsi) at temperatures up to 300°C. However, these experiments are beyond the scope of the present study.

It can also be expected that there would be a statistical variation in the output of nominally identical devices due to the natural variation in powder column microscopic properties such as the small, unavoidable local variations in density, porosity, stoichiometry, thermal properties, etc. The initial transition to convective burning occurs at a microscopic site which may occur at slightly different points into the burn for different powder columns. Differences in powder compaction ahead of the burn may also effect the way the unburned column reacts to the burn front. Variations in the pressure at which a closure disk ruptures could also effect the output. It has even been observed that smaller amounts of powder loads can increase the impulse from a component due to the larger powder porosity and quicker transitions to convective burning.[38]

BOMB CALORIMETRY

The calorific output of OEA batch TR120591 was measured in Mound's bomb calorimetry facility. The standard procedure is to measure the output of four 250 mg pellets. The outputs of four pellets ranged from 1546.60 to 1555.40 cal/g with an average of 1551.09 cal/g and a standard deviation of 4.24 cal/g. The output is similar to $TiH_{1.65}/KClO_4$. Mound's blend PC-193 had an output of 1559.13 $\pm$ 2.25 cal/g.

FIXED VOLUME FIRINGS OF PRESSURE CARTRIDGE ASSEMBLY

Experimental

Three fully loaded pressure cartridge assemblies, P/N SKD26100098-301, were received from NASA. Each cartridge contains 13.2 gms of $TiH_2/KClO_4/Viton$ with a NASA Standard Initiator (NSI) mounted in the bottom as the ignition source. The cartridges were manufactured by OEA of Denver, Colorado, in June, 1991 and are from batch HBK with serial numbers 00021, 00047, and 00048.

A chamber was constructed to measure the pressure-time output of a single pressure cartridge assembly. A cross section of the chamber is shown in Figure 13. It is constructed of 316 stainless steel and has an overall diameter of 21.6 cm(8.5 inches) and a height of 12.7 cm(5 inches). The volume into which the cartridge fires simulates the initial volume in the shear bolt assembly. It was decided to add the liner after the main body was constructed, and the inner diameter of the liner is 11.10 cm(4.37 inches) compared to the 11.43 cm(4.5 inches) in the shear bolt assembly. The lip of the liner is 0.132 cm(0.052 inches) high, the same as the initial distance of the piston above the assembly base. Two cartridges were fired with this size liner in the vessel. The third cartridge was fired with a liner that creates a smaller internal volume so that a higher pressure would be generated. The second liner has the same 0.132 cm depth lip. However, the lip is formed by a 7.62 cm(3 inch) diameter circle centered 1.75 cm(11/16 inch) from the cartridge center toward the transducer. In the cross section of Figure 13, the second liner would be solid up to the O-ring plate in the region left of the cartridge. The purpose of a liner is to take the brunt of the damage produced by the cartridge so that only a liner and the O-ring plate would have to be replaced after each shot, and the main chamber body would have minimal damage.

The top of the cartridge is 0.671 cm(0.264 inches) from the top of the liner base, the same as in the shear bolt assembly.

The volumes contained in the fixed volume vessel with the larger and smaller liner are tabulated and compared to those in the shear bolt assembly in Table 3. The volumes are indicated in Figure 14. Volume L is the volume contained between the liner base and the O-ring plate, volume A is the volume between the cartridge top and liner base, and volume C is the volume in a cartridge.

TABLE 3. The volumes contained in the fixed volume vessel as indicated in Figure 14 and the shear bolt assembly initial volume. The shear bolt assembly volume contains the volumes above and in two cartridges.

Volume	Larger Liner cm³ (in³)	Smaller Liner cm³ (in³)	Shear Bolt Assembly cm³ (in³)
L	12.77 (0.780)	6.02 (0.367)	13.55 (0.827)
A	3.53 (0.216)	3.53 (0.216)	3.53 (0.216)
C	6.42 (0.392)	6.42 (0.392)	6.42 (0.392)
L + A	16.3 (0.996)	9.55 (0.583)	20.6 (1.26)
L + A + C	22.7 (1.39)	16.0 (0.975)	33.5 (2.04)

The firing volume is sealed with the O-ring on the cartridge and the O-ring in the groove on the vessel bottom. This latter O-ring is compressed by the O-ring plate when the vessel cover is screwed down. The O-ring has a 5 inch outer diameter with a 1/8 inch wall, and is made from ethylene propylene, the same material as the O-rings in the shear bolt assembly. When the vessel cover is tightened on the O-ring plate, it can be felt to bottom out on the O-ring groove and liner.

A vent hole placed beyond the O-ring releases any pressure that leaks past the O-ring.

A Kistler 207C pressure transducer is mounted 4.45 cm(1.75 inches) from the center of the pressure cartridge. The transducer output is amplified by a Kistler 504E amplifier with a 545A15 filter. This filter extends the amplifier's frequency response to 1 MHz. The transducer has a rise time specification (10 - 90% points) of 1.5 μsec. The pressure waveform generated during a burn is recorded on an Analogic Data Precision 6000A waveform recorder as previously described.

Initial testing of the vessel was conducted with an adapter fitting in place of the pressure cartridge. This fitting mounted into the same location as the cartridge with the same O-ring seal, and contained threads to fit to a standard high pressure rupture disk assembly. The rupture disk assembly was connected to the high pressure system so that pressurizing the adapter past the rating of the rupture disk would burst the disk and cause a pressure pulse into the vessel volume. A 3,000 psi and a 20,000 psi rupture disk were burst with this setup. The pressure pulses from these bursts were recorded on the waveform recorder thus assuring the proper operation of the transducer and recording system and the integrity of the vessel and O-ring seals.

The NSI was ignited with a 5 amp, 3 millisecond constant current pulse.

The waveform recorder has the capability of recording the same input with two different time bases. All three cartridge pressure waveforms were recorded with a period of 1 μsec for 4,096 points for a total recording time of 4 msec. Additionally, the first shot was

recorded with a 20 μsec period and the second and third shots at 1 msec periods for 4,096 points for total recording times of 81 msec and 4 seconds, respectively.

After each shot, the cover was difficult to remove even though the threads had been liberally coated with an anti-galling lubricant. It was necessary to use a chain wrench to loosen the cover, but once it was loosened, it screwed out very easily.

Cartridge Pressure Traces

The pressure traces of the two cartridges (serial numbers 00047 and 00048) fired into the 16.3 cm^3 volume are shown with an expanded time scale in Figure 14, and over the full 4.1 msec recorded with the 1 μsec period in Figure 15. The two pressure traces are very similar with a flattening of the pressure rise occurring 90-100 μsec into the burn before a few very similar oscillations occur. The 90-100 μsec may be considered the time it takes for a cartridge to deliver its pressure across the initial volume of the shear bolt assembly. The maximum pressures developed at the peaks of the oscillations were 26,350 psi for both cartridges. Immediately after the initial spiking, at about the 1.07 msec point in Figure 14, the pressure was about 21,500 psi in the upper trace and 20,900 psi in the lower trace. Two cartridges firing into the same volume would produce more than twice the pressure of one cartridge because the temperature should be higher.

The pressure trace of the cartridge (serial number 00021) fired into the 9.55 cm^3 volume is shown in Figure 16 with an expanded time scale and over the full 4.1 msec recorded with the 1 μsec period in Figure 17. The maximum pressure reached was 33,460 psi, with an abrupt decrease to about 18,000 psi which is probably the result of failure of the 5 inch O-ring seal. If the internal volume of the cartridge is not used to calculate the total free volume and the pressure from this shot had scaled as the ratio of the two liner volumes (1.7), a maximum pressure of 44,800 psi would be predicted from the larger liner volume. If the internal cartridge volume is used, the volume ratios (1.4) would predict a maximum pressure of 37,500 psi.

The pressure traces recorded with the 1 msec period are shown in Figures 18 and 19. It can be seen that the pressure has decayed to near its final value in about 0.4 to 0.5 seconds. Most of this decay is probably due to condensation of reaction products although some of it is due to leaks past the 5 inch O-ring as discussed in the next section.

O-Ring Leaks

Before each shot, a piece of tape was placed over the vent hole. If there was a leak through the vent hole, the tape would be blown off as an indicator. The tape was blown off the vent hole in all three shots. In addition, a sound indicative of a high pressure leak could be heard through the door of these remotely fired shots. There seemed to be a delay between ignition and the sound for the larger volume liner shots, but the sound seemed almost instantaneous with ignition for the smaller liner volume shot. The initial impulse from the cartridge may have moved the O-ring plate slightly thereby decreasing the strength of the seal.

When the cartridge was removed after firing, there was no pressure release in the first

shot, 00048, but there was pressure release after the second, 00047, and third, 00021, shots. After disassembly of the vessel, it was found that the O-ring was burned through on the first shot but not on the second and third. In the latter two shots, the O-ring probably leaked at the highest pressures reached, but then resealed after some pressure release.

The first shot, 00048, was recorded at the long time interval of 20 μsec for a total time of 81 msec. There was no structure in this pressure trace or the one in Figure 14 out to 4 msec that would indicate an abrupt pressure release. However, when compared to the following two shots, 00047 and 00021, the pressure decayed quicker when there was a burn through of the O-ring.

A high pressure leak in the O-ring in the second shot, 00047, may have occurred at the approximately 3,000 psi pressure decrease near the 1.10 msec point in Figures 14 and 15, with the subsequent small amplitude-long period oscillations indicating a resealing. A similar smaller leak may have occurred in the first shot at about the same time as indicated by a smaller pressure oscillation in Figure 15. In the third, smaller volume shot, shown in Figure 16, a leak definitely occurred at the 0.93 msec point, due to the approximately 16,000 psi pressure decrease and failure to reach the expected 44,800 psi. The subsequent "resealing" oscillations are more apparent in Figures 16 and 17 and occur around 20,000 psi as in Figure 15. It appears that about 20,000 psi may be the fundamental long-time sealing limit of the O-ring seal in this configuration in the vessel.

The pressure traces seem to indicate whether there has been an O-ring burn through or just a leak. A burn through is indicated by a faster pressure decay in Figure 18. Leaking and resealing seem to be indicated by small oscillations with a period of about 300 μsec in Figures 15 and 17.

Post mortem of vessel

Photographs of the vessel interior were taken after the first shot. The appearance of the vessel interior after the second and third shots was very similar, with the exception of no O-ring burn through occurring on these shots.

The interior of the vessel with the liner removed is shown in Figure 20. The screw in the vessel base aligns with one of two holes in the liner to ensure that the second hole remains over the transducer during assembly. The pressure transducer can be seen near the top of the vessel base. A significant amount of the reaction products had condensed between the bottom of the liner and the vessel base.

Figure 21 compares an unused liner to the one used in the first shot. It can be seen how the reaction products have been pushed out to the liner perimeter by the higher pressure in the center.

Figure 22 is a closeup of the liner showing how it has been somewhat eroded near the center and bent. There was an overall twist to the liner and a somewhat concentric upward bulge at a diameter of about 2 3/4 inches. The liners after the first two shots were very similar in appearance. The smaller liner used for the third shot was similarly distorted, but the distortion was confined in the open volume section of the liner.

Figure 23 shows the O-ring plate after the first shot. The O-ring tended to stick in its groove and to the plate after a shot, and the O-ring plate was gently tapped through the

cartridge hole to release it. A thin black residue on the plate and O-ring groove was probably caused by a little charring of the O-ring along is edges.

Figure 24 shows the burn through of the O-ring at the O-ring plate surface after the first shot. A small channel which has been cut by the hot reaction products can be seen in the O-ring plate. The roughening of the O-ring surface from being exposed to the heat can also be seen. The vessel was constructed with the purpose of measuring the pressure output of a cartridge, and it was fortuitous that we were able to somewhat simulate the burn through of the O-ring.

The O-rings from the second and third shots left some charring on the O-ring plate and O-ring groove and had some damage on the outer diameter, but there did not appear to be any locations on them where it looked like a burn through was about to occur.

Figure 25 shows the O-ring plate after it has been cleaned. In the center, an outline of the cartridge diameter can be seen. This circular region is slightly below the surface of the rest of the plate. It could be a dent from the initial pressure burst from the cartridge and/or erosion damage from its direct line of sight to the high pressure reaction products. The dark large circle on the plate is at the location of the inner diameter of the liner lip. It is actually a small groove that has been cut into the plate.

The condition of these pieces after a shot is consistent with what would be intuitively expected. The initial burst of pressure from the cartridge closure disk rupture would occur at the center. The pressure gradient from the center to edge would then push the hot reaction products to the liner lip. This is exactly where the highest concentration of products were observed in Figures 21 and 22. The damage at the center of the O-ring plate also indicates that the plate would receive a rather large impulse whether it was sealed or not.

CONCLUSIONS

The burn rate behavior of OEA batch TR120591 $TiH_2/KClO_4/Viton$ is generally "well behaved" in the sense that there were no acoustically-driven flame instabilities or abrupt pressure increases due to any burn transitions over the pressure range investigated. If any instabilities or abrupt pressure increases were observed, it could be argued that they could occur at different points in a burn due to microscopic statistical variations in the homogeneity of a pellet. The occurrence of such a transition in a burn could cause the pressure output of a pellet to be higher if the transition occurred earlier in a burn; the higher pressures in these pellets could be responsible for the O-ring blow-by. However, the higher hydrogen content and/or the Viton seem to inhibit these transitions when compared to our previous results on the $TiH_{1.65}/KClO_4$ system. There does not seem to be any inherent peculiar burn characteristic of $TiH_2/KClO_4/Viton$ (at least for batch TR120591) that could cause an anomalously high pressure output and subsequent O-ring blow-by in the forward shear bolt assembly.

The fitted parameters a and n are useful as batch characterization parameters, with n generally being the index which is used for comparison.[2] The measurement reported here provide baseline values for a and n. Comparisons could be made with different batches or with dependencies on particle size, mass ratio changes, aging, etc. Different batches, particularly those with different particle size distributions, may also show different pressures

and intensities of the conductive-to-convective burning transition. Such changes could cause variations in the pressure output of a cartridge.

The firings of the three SKD26100098-301 pressure cartridges into fixed volumes were initially planned to measure the pressure outputs of the cartridges, but more information can be inferred from the results. The two cartridges fired into the same volume produced almost identical outputs as seen in Figures 14 and 15. Although this is only two data points, it does provide more confidence in the reproducibility of the outputs from the pressure cartridges than if the outputs were different. The O-ring sealing technique used in the fixed volume vessel is probably not as good as that used in the shear bolt housing. The shear bolt housing uses two O-rings with backup rings. The vessel O-ring seal seemed to have a pressure limit of about 20,000 psi although much higher pressures are briefly measured. A leak at the O-ring in the vessel might possibly occur very rapidly from the initial impulse from the cartridge on the O-ring plate. The O-ring seals on the side on the piston in the shear bolt assembly would not experience this effect. The leaking of the O-ring seal in the vessel provided information about some of the effects of an O-ring leak. The pressure traces showed that a maximum pressure is reached in about 100 μsec after the cartridge closure disk rupture. Thus, significant pressures can be achieved in the fixed volume even if there are O-ring leaks; the pressure is generated much more rapidly than it can dissipate through an O-ring leak. This rapid pressure buildup coupled with the O-ring plate damage directly above the cartridge implies that the piston in the shear bolt assembly will receive a very large impulse from the two pressure cartridges. The initial impulse received directly above each cartridge could even possibly be enough to move the piston without much confinement of the resulting pressure.

It has been shown that a fixed volume chamber can be used to measure the pressure-time outputs of the pressure cartridges, and that the vessel can be used to simulate O-ring leaks. Variations of the vessel used in these measurements with more instrumentation could more closely simulate the O-ring sealing in the shear bolt assembly and provide even more information about the effects of O-ring leaks.

ACKNOWLEDGEMENTS

REFERENCES

1. Reed, J. W., *Equilibrium Real Gas Thermodynamics Computations for the System TiH₂/KClO₄/Viton-B*, MLM-   , EG&G Mound Applied Technologies, to be published.

2. Juhasz, A. A. and C. F. Price, *The Closed Bomb Technique for Burning Rate Measurement at High Pressure*, in <u>Experimental Diagnostics in Combustion of Solids, Progress in Astronautics and Aeronautics, Vol. 63</u>, edited by T. L. Boggs and B. T. Zinn (American Institute of Aeronautics and Astronautics, 1978), p. 129.

3. Kubota, N., *Survey of Rocket Propellants and Their Combustion Characteristics*, in <u>Fundamentals of Solid-Propellant Combustion, Progress in Astronautics and Aeronautics, Vol. 90</u> edited by K. K. Kuo and M. Summerfield (American Institute of Aeronautics and Astronautics, 1984), p. 1.

4. Shimpi, S. A. and H. Krier, *The Closed Bomb Test for the Assessment of Solid Propellant Grains*, Combust. Flame <u>25</u>, 229 (1975).

5. Constantino, M. and D. Ornellas, *A Hybrid Closed Bomb-Strand Burner for Very High Pressure Burning Rate Measurements*, <u>23rd JANNAF Combustion Meeting, Vol. I</u>, CPIA Publication 457 (1986), p. 307.

6. Tao, W. C., M. S. Constantino, and D. L. Ornellas, *Burning Rates of Two Cast Nitramine Explosives Using a Hybrid Closed Bomb-Strand Burner*, <u>Proceedings of the Ninth Symposium (International) on Detonation</u> (Portland, Oregon, 1989), p. 1310.

7. Conkling, J. A., <u>Chemistry of Pyrotechnics</u> (Marcel Dekker, Inc., 1985), p. 114.

8. McLain, J. H., <u>Pyrotechnics</u>, (The Franklin Institute Press, 1980), p. 59.

9. Ward, J. R., L. J. Decker, and A. W. Barrows, *Burning Rates of Pressed Strands of a Stoichiometric Magnesium-Sodium Nitrate Mix*, Combust. Flame <u>51</u>, 121 (1983).

10. Lessard, P., D. Sanschagrin, and G. Couture, *A Review of Recent Work at DREV on Castable Smoke Compositions*, <u>Proceedings of the Ninth International Pyrotechnics Seminar</u>, (Colorado Springs, Colorado, 1984), p. 349.

11. Timnat, Y. M., *Pyrotechnics Research in Israel*, ibid., p. 637.

12. Durgapal, U. C. and A. R. Menon, *Studies on Tantalum-Potassium Dichromate Pyrotechnic System*, <u>Proceedings of the Fifteenth International Pyrotechnics Seminar</u>, (Boulder, Colorado, 1990), p. 221.

13. Hasue, K., A. Iwama, and T. Kazumi, *Further Investigation of the Combustion Aspects*

of Sodium Azide, Potassium Perchlorate, and Burning Rate Catalyst Mixtures, <u>Proceedings of the Sixteenth International Pyrotechnics Seminar</u>, (Jönköping, Sweden, 1991), p. 57.

14. Holy, J. A., *Pressure Dependent Burn Rates of $TiH_x/KClO_4$ (x=0.2, 0.65, 1.65)*, <u>Proceedings of the Eleventh International Pyrotechnics Seminar</u>, (Vail, Colorado, 1986), p. 327.

15. Dobratz, B. M., <u>LLNL Explosives Handbook</u>, UCRL-52997(1981), p. 19-145.

16. Robertson, M. M. and E. A. Igel, *High Speed Optical Studies of Pyrotechnic Initiation Phenomena*, <u>Proceedings of the Fifth International Pyrotechnics Seminar</u>, (Vail Colorado, 1976), p. 485.

17. Holy, J. A., *Laser Initiation of $TiH_x/KClO_4$ (x=0.2, 0.65, 1.65)*, <u>Proceedings of the Eleventh International Pyrotechnics Seminar</u>, (Vail, Colorado, 1986), p. 313.

18. Holy, J. A. and T. C. Girmann, *The Effects of Pressure on the Laser Initiation of $TiH_x/KClO_4$ and Other Pyrotechnics*, <u>Proceedings of the Thirteenth International Pyrotechnics Seminar</u> (Grand Junction, Colorado, 1988), p. 449.

19. Belyaev, A. F., V. K. Bobolev, A. I. Korotov, A. A. Sulimov, and S. V. Chiuko, <u>Transition from Deflagration to Detonation in Condensed Phases</u> (Izdatel'stvo "Nauka", Moscow, 1973); English translation available from NTIS, TT-50028 (1975).

20. Velicky, R. W. and J. Hershkowitz, *Anomalous Burning Rate Characteristics of Composition B and TNT*, <u>Seventh Symposium (International) on Detonation</u>, (Annapolis, Maryland, 1981), p. 428.

21. Holy, J. A., *Burn Rates of Explosives at High Pressures*, <u>Proceedings of the American Defense Preparedness Association Joint Symposium on Compatibility of Plastics and Other Materials with Explosives, Propellants, and Pyrotechnics and Processing of Explosives, Propellants, and Ingredients</u>, (Hilton Head Island, South Carolina, 1985), p. 124.

22. Hingorani-Norenberg, S. L., *An Experimental Study of the Burn Rate of $TiH_{1.65}/KClO_4$ Pyrotechnic Under Confinement*, Sandia National Laboratory Report SAND88-2393 (1988).

23. Hingorani-Norenberg, S. L. and L. M. Moore, *Preliminary Burn Rate Studies on $TiH_{1.65}/KClO_4$*, <u>Proceedings of the Thirteenth International Pyrotechnics Seminar</u>, (Grand Junction, Colorado, 1988), p. 899.

24. Hingorani-Norenberg, S. L., A. Razani, and M. Shahinpoor, *Compaction of $TiH_{1.65}/KClO_4$ Pyrotechnic Powder During Confined Burn*, <u>Proceedings of the Fifteenth International Pyrotechnics Seminar</u>, (Boulder, Colorado, 1990), p. 221.

25. Langellé, G., A. Biyot, J. D. Duterque, and T. F. Trubert, *Steady-State Burning of Homogeneous Propellants*, in Fundamentals of Solid-Propellant Combustion, Progress in Astronautics and Aeronautics, Vol. 90 edited by K. K. Kuo and M. Summerfield (American Institute of Aeronautics and Astronautics, 1984), p. 361.

26. Ramohalli, K. N. R., *Steady-State Burning of Composite Propellants under Zero Cross-Flow Situation*, in Fundamentals of Solid-Propellant Combustion, Progress in Astronautics and Aeronautics, Vol. 90 edited by K. K. Kuo and M. Summerfield (American Institute of Aeronautics and Astronautics, 1984), p. 409.

27. Williams, F. A., Combustion Theory (The Benjamin/Cummings Publishing Company, Inc., 1985), p. 232.

28. Price, E. W., *Combustion of Metalized Propellants*, in Fundamentals of Solid-Propellant Combustion, Progress in Astronautics and Aeronautics, Vol. 90 edited by K. K. Kuo and M. Summerfield (American Institute of Aeronautics and Astronautics, 1984), p. 479.

29. Östmark, H. and N. Roman, *Laser Ignition of Pyrotechnic Mixtures: Ignition Mechanisms*, J. Appl. Phys. **73**, 1992 (1993).

30. Erickson, K. L., *Effect of Oxide Coating Thickness on Thermal Ignition of Titanium-Based Pyrotechnics*, Proceedings of the Ninth International Pyrotechnics Seminar, (Colorado Springs, Colorado, 1984), p. 799.

31. Erickson, K. L., J. W. Rogers, Jr., and S. J. Ward, *Titanium Oxidation Kinetics and the Mechanism for Thermal Ignition of Titanium-Based Pyrotechnics*, Proceedings of the Eleventh International Pyrotechnics Seminar, (Vail, Colorado, 1986), p. 679.

32. Erickson, K. L., J. W. Rogers, Jr., and R. D. Skocypec, *Thermal Ignition of Ti-Based Pyrotechnics II. Ti Oxidation Kinetics Applied to Analysis of Slow (DTA) Experiments*, Proceedings of the Twelfth International Pyrotechnics Seminar, (Juan-les-Pins, France, 1987).

33. Nelson, L. S., D. E. Rosner, S. C. Kurzius, and H. S. Levine, *Combustion of Zirconium Droplets in Oxygen/Rare Gas Mixture - Kinetics and Mechanisms*, Twelfth Symposium (International) on Combustion (The Combustion Institute, Pittsburgh, Pennsylvania, 1969), p. 59.

34. Collins, L. W., *Thermal Ignition of Titanium Based Pyrotechnics*, Combust. Flame **41**, 325 (1981).

35. Moddeman, W. E., L. W. Collins, P. S. Wang, and T. N. Wittberg, *Role of Surface Chemistry in the Ignition of Pyrotechnic Materials*, Proceedings of the Seventh International Pyrotechnics Seminar, (Vail, Colorado, 1980), p. 408.

36. Wang, P. S., T. N. Wittberg, J. D. Wolf, and R. G. Keil, *Oxygen Diffusion of Anodic Surface Oxide Films on Titanium Studied by Auger Electron Spectroscopy*, Proceedings of the Eighth International Pyrotechnics Seminar, (Steamboat Springs, Colorado, 1982), p. 693.

37. Wang, P. S., T. N. Wittberg, J. D. Wolf, and R. G. Keil, *Oxygen Diffusion from Anodic Surface Oxide Films on Titanium Subhydride Studied by Auger Electron Spectroscopy and Electron Energy Loss Spectroscopy*, Proceedings of the Ninth International Pyrotechnics Seminar, (Colorado Springs, Colorado, 1984), p. 685.

38. Munger, A. C., private communication.

APPENDIX I. Pressure and Burn Rate Values

Table AI.1. The initial pressure, average pressure, and burn rate values of $TiH_2/KClO_4/Viton$, OEA Lot TR120591, in nitrogen. The average pressure and burn rate are used in the burn rate vs. pressure plots.

Initial Pressure (MPa,abs)	Average Pressure (MPa,abs)	Burn Rate (cm/sec)	Initial Pressure (MPa,abs)	Average Pressure (MPa,abs)	Burn Rate (cm/sec)
0.100	0.155	0.759	69.119	70.332	13.833
0.183	0.279	1.166	82.909	84.205	13.622
0.410	0.679	1.773	103.525	104.801	14.960
0.803	1.217	2.198	117.384	118.701	15.732
1.479	1.975	2.852	138.000	139.386	16.817
2.100	2.624	3.230	138.276	139.662	15.937
2.879	3.437	3.654	143.171	144.488	16.215
3.610	4.203	4.047	151.790	152.921	16.875
4.727	5.361	4.603	172.475	173.895	17.294
11.132	11.884	6.015	206.950	208.267	18.487
13.890	14.683	7.257	245.562	246.665	18.403
20.785	21.592	8.771	278.520	279.596	20.644
34.644	35.609	10.742	310.375	311.540	19.279
48.365	49.420	12.242			

Figure Captions

Figure 1. A cross section of the pressure bomb and sample mounting used for measuring burn rates. S.S. = stainless steel.

Figure 2. The change in pressure resulting from burning samples with initial pressures of N_2 of 5, 10, and 15 Kpsi (34.5, 68.9, and 103 MPa).

Figure 3. The change in pressure resulting from burning samples with initial pressures of N_2 of 418, 524, and 686 psia (2.88, 3.61, and 4.73 MPa).

Figure 4. The change in pressure resulting from burning samples with initial pressures of N_2 of 15 and 27 psia (103 and 186 KPa).

Figure 5. The change in pressure resulting from burning samples with initial pressures of N_2 of 30, 40.4, and 45 Kpsi (207, 279, and 310 MPa). The arrow at the 45 Kpsi trace indicates the division between two approximately linear sections with different slopes.

Figure 6. The burn rate of $TiH_2/KClO_4/Viton$ lot TR120591 as a function of pressure in nitrogen.

Figure 7. A model of a burning solid from Williams.[26]

Figure 8. a) SEM of $TiH_2/KClO_4/Viton$, lot TR120591, at 250 magnification, b) at 500 magnification, c) EDAX map of Ti, d) EDAX map of K + Cl.

Figure 9. Product residue from a burn in 290 psi of nitrogen. a) SEM at 500 magnification, b) Ti EDAX map, c) K + Cl EDAX map, d) SEM at 3000 magnification.

Figure 10. a) and b) Product residue from a burn in 45 psi of nitrogen.

Figure 11. Product residue from a burn in 20,750 psi of nitrogen. a) SEM at 200 magnification, b) Ti EDAX map, c) K + Cl EDAX map.

Figure 12. SEM at x10 magnification of product residue from a burn at 45 Kpsi.

Figure 13. A cross section of the fixed volume vessel used to measure the output of the NASA SKD26100098-301 pressure cartridge. NSI = NASA Standard Initiator.

Figure 14. The various volumes in the vessel of Figure 13. Volume L is the volume between the liner base and O-ring plate, volume A is the volume between the top of the cartridge and the liner base, and volume C is the volume in the cartridge.

Figure 15. Pressure traces of the two cartridges with serial numbers 00047 and 00048 fired

into a fixed volume of 16.3 cm^3(0.996 in^3) on an expanded time scale. 00048 has been shifted by +10 Kpsi for clarity.

Figure 16. Pressure traces of Figure 14 over the whole 4.1 msec recording time. 00048 has been shifted by +10 Kpsi for clarity.

Figure 17. Pressure trace of cartridge 00021 fired into a fixed volume of 9.55 cm^3 on an expanded time scale.

Figure 18. Pressure trace of Figure 16 over the whole 4.1 msec recording time.

Figure 19. Pressure traces of 00047 and 00048 cartridges recorded with longer time periods than in Figures 14 and 15.

Figure 20. Pressure traces of two cartridges recorded with a 1 msec time period fired into the 16.3 cm^3 fixed volume (00047) and the 9.55 cm^3 fixed volume (00021).

Figure 21. The interior of the vessel after the first shot with cartridge 00048.

Figure 22. A comparison of the liner before and after the first shot.

Figure 23. A closeup of the liner showing how it has been bent.

Figure 24. The side of the O-ring plate facing the cartridge after a shot.

Figure 25. A hole in the O-ring and groove in the O-ring plate caused by the burn of cartridge 00048.

Figure 26. Damage to the O-ring plate after the first shot. The groove at the left edge is the same groove that is at the O-ring hole in Figure 24.

Pressure
Bomb

Pressure
Transducer

S.S. Shield

Ignition
Wire

Sample

S.S. Inserts

Electrical
Feedthroughs

Fig. 1

Fig. 2

TIME (msec)

0   20   40   60   80   100   120

−100

0

100

200

300

400

500

Δ PRESSURE (psi)

5 Kpsi

10 Kpsi

15 Kpsi

Fig. 4

Fig. 5

TIME (msec)

0   10   20   30   40   50   60   70   80   90

45 Kpsi

40.4Kpsi

30 Kpsi

Δ PRESSURE (psi)

0   100   200   300   400   500

Fig. 6

PRESSURE (MPa)

BURN RATE (cm/sec)

$R=2.05P^{.472}$

$R=4.38P^{.266}$

Fig. 7

X500 2.1 TiH2/KClO4 Viton K2CL

X500 8u) TiH2/KClO4 Viton Ti

X500 8u) TiH2/KClO4 Viton

X250 8u) TiH2/KClO4 Viton

9 b

X500 9 b) NTHKA 18 Ti

9 d

X3000 9 d) NTHKA 18
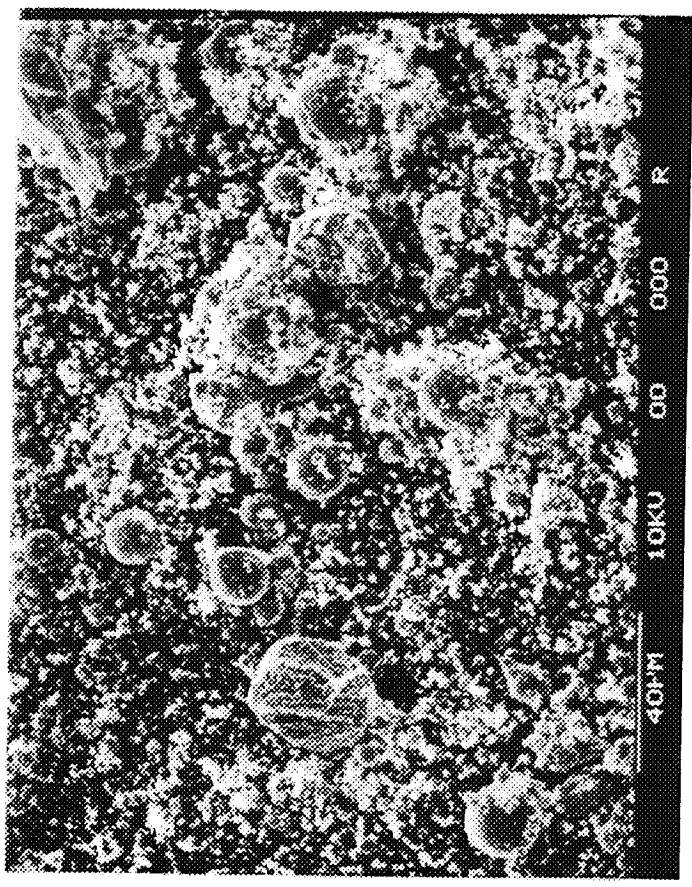
X500 9 a) NTHKA 18

X500 9 c) NTHKA 18 K, Cl

10 b

NTHKA 21   10KU   OOO   R

X3000   (10b)

NTHKA 21   10KU   OO   OOO   R

X3000   (10a)

11b)

11c

X200 11b) NTHKA 24   Ti

X200 11a) NTHKA 24

X200 11c) NTHKA 24   KCl

Fig. 12

Vessel Cover

Mounting Plate

Vessel Body

Vent Hole

O-Ring Plate

O-Ring

Liner

Pressure Transducer

NASA Pressure Cartridge

O-Ring

NSI

Figure 13

L

A

C

Fig. 14

Fig. 15

PRESSURE (Kpsi)

TIME (msec)

00047

00048

Fig. 16

00021

PRESSURE (Kpsi)

TIME (msec)

Fig. 17

Fig. 18

TIME (msec)

90 80 70 60 50 40 30 20 10 0

PRESSURE (Kpsi)

0

10

20

00048

00047

Fig. 21

Fig. 22

Fig. 23

Fig. 24

Fig. 25

Fig. 26